Hot deformation behavior and constitutive modeling of VCN200 low alloy steel

A. Momeni [a,*], S.M. Abbasi [b], H. Badri [c]

[a] Department of Materials Science and Engineering, Hamedan University of Technology, Hamedan, Iran
[b] KNT University of Technology, Tehran, Iran
[c] Tarbiat Modarres University, Tehran, Iran

ABSTRACT

The hot working behavior of VCN200 medium carbon low alloy steel was analyzed by performing hot compression tests in temperature range of 850–1150 °C and at strain rates of $0.001–1\ s^{-1}$. Flow curves were typical of dynamic recrystallization during hot working over temperature range of 900–1150 °C and strain rates of $0.001–1\ s^{-1}$. However, at lower temperatures no indication of flow softening was observed. The constitutive analysis using the hyperbolic sine function was performed and the value of apparent activation energy for the hot deformation determined to be about 435 kJ/mol. The flow curves up to the peak were successfully modeled using a dynamic recovery model. All the factors in this model were defined in terms of the Zener–Hollomon parameter. A modified form of Avrami equation was used to estimate the fractional softening due to the dynamic recrystallization for any given strain in flow curve. Using this model, the flow curves were successfully predicted and generalized to different deformation conditions.

© 2012 Elsevier Inc. All rights reserved.

1. Introduction

Hot deformation of an alloy is often analyzed from the flow curves obtained at high temperature testing as well as the corresponding microstructural evolutions. A prosperous design of an industrial hot working process is ensured by acquiring a deep knowledge about the microstructural evolution of the alloy and by defining the dependence of flow curve to the deformation variables, i.e. strain, strain rate and temperature. Many of previous researchers have worked to establish different constitutive equations between flow stress and deformation parameters. Many of these works have been devoted to determine the material constants in previously well-developed constitutive equations for the hot deformation of different industrial alloys [1–5]. Some other researchers proposed their own formulas to model a typical hot flow curve. It has been observed that the flow stress can be defined as the multiplication individual functions each one describing the dependence to a deformation variable [6]. Irrespective of the fact that the different constitutive equations have been developed based on the phenomenological or experimental concepts, they have been used to generalize the laboratory data to actual industrial hot working processes. Therefore, proposing a constitutive equation which opens a way to predict the flow stress of a given material in an industrial process such as hot rolling or forging is still of great interest.

Many investigations have declared that dynamic recrystallization is the major microstructural phenomenon during hot deformation of carbon, low alloy and stainless steels [7–11]. This is because austenite in steels has low stacking fault energy

---

* Corresponding author. Tel.: +98 21 9123349007.
  E-mail address: ammomeni@aut.ac.ir (A. Momeni).

which decreases the efficiency of dynamic recovery [12,13]. During hot deformation, DRX starts once the build-up of dislocations reaches a critical value [14,15]. The softening due to DRX gives rise to decreasing flow stress and leaves a peak on the flow curve. However, DRX actually starts at a critical strain, ε_c which is 0.6–0.8 times the peak strain, ε_p [16,17]. Beyond the peak, softening keeps on to a dynamic balance with work hardening which is attained in the plateau of steady state deformation.

Medium carbon low alloy steels are greatly applicable alloys which are used in many different industrial applications. Although they are prepared by quenching and tempering treatments, the high temperature deformation of theses alloys to the finished or semi-finished products have drawn little attentions. The present work is therefore devoted to address the hot deformation behavior of VCN200 medium carbon low alloy steel.

2. Experimental procedures

The material used in this investigation was VCN200 medium carbon low alloy steel having the composition of 0.29% C, 0.38% Si, 0.55% Mn, 1.97% Cr, 2.20% Ni, 0.34% Mo, 0.06% Ti, 0.34% Cu, 0.015% P, 0.004% N and the balance of Fe (in wt%). Cylindrical compression samples of 10 mm height and 15 mm diameter were prepared from the as-received hot forged bar. Graphite was used to reduce friction between the contacting surfaces of samples and anvils. An Instron 8502 testing machine, equipped with a fully computerized furnace, was used to perform hot compression tests. Before testing, all the specimens were reheated at 1200 °C for 30 min, followed by cooling down and soaking about 10 min at deformation temperature. Continuous hot compression tests were carried out in a temperature range of 850–1150 °C with the intervals of 50 °C and at strain rates of 10^{-3}–1 s^{-1}.
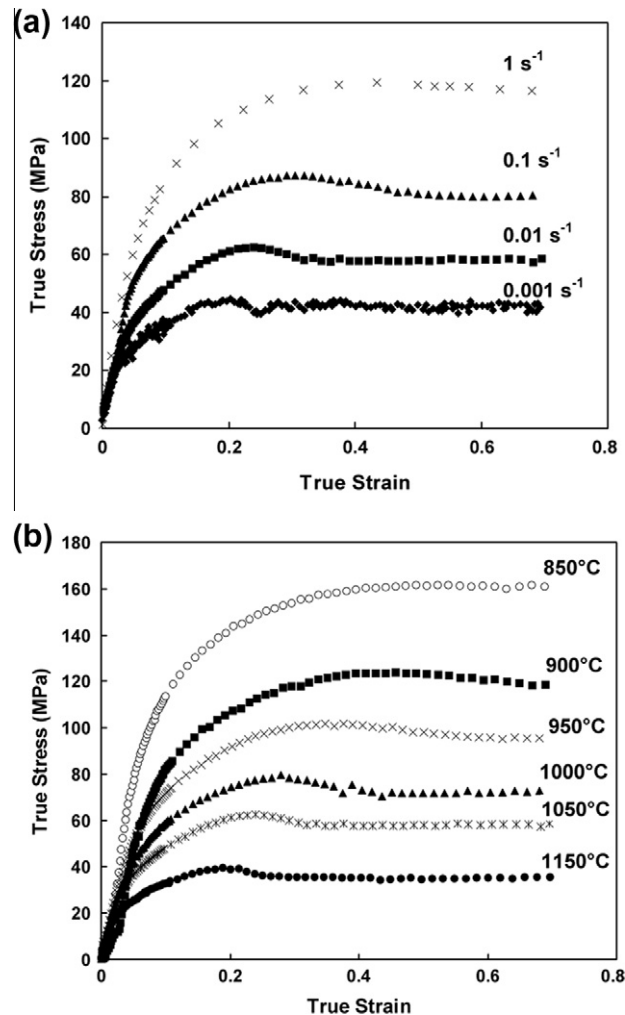

Fig. 1. Typical DRX flow curves obtained at different deformation conditions. (a) 1050 °C, (b) 0.01 s^{-1}.

3. Results and discussion

Some representative flow curves of the studied steel at different deformation conditions are shown in Fig. 1. This figure indicates the influence of strain rate, Fig. 1(a), and deformation temperature, Fig. 1(b), on the flow curves. As expected, flow stress level increases with increasing temperature and decreasing strain rate. Also the typical form of a DRX flow curve is more observable at high temperatures and low strain rates. At high strain rates or low temperatures, concurrent deformation decelerates the rate of work softening giving rise to a more faded peak. In this case, peak point and the onset of steady state flow are also shifted to higher strain levels. Although most of flow curves indicate a single peak, the multi-peak behavior is also discernible at low strain rates and high temperatures. When the recrystallization strain $\varepsilon_x = \varepsilon_s - \varepsilon_p$ is lower than ε_p (ε_p is peak strain and ε_s is steady state strain), nucleation is cyclic in nature and the growth rate of new grains is higher than their nucleation rate. In such a case, a cycle of DRX is completed before the next starts and the flow curve is multi-peak in nature. On the other hand, when $\varepsilon_x > \varepsilon_p$, recrystallization becomes continuous because the strain required for nucleation is smaller than that needed for growth [18]. Consequently, the material is partially recrystallized and the successive cycles of nucleation overlap so that a single-peak flow curve appears.

In order to model the flow curves of DRX, the first step is to determine the value of apparent activation energy of the material. The basic equation often used for the determination of the apparent activation energy, Q, is as follows:

$$Z = \dot{\varepsilon} \exp\left(\frac{Q}{RT}\right) = A[\sin h(\alpha \cdot \sigma)]^n, \tag{1}$$

where Z is the Zener–Hollomon parameter and α, A and n are material constants. Eq. (1) embraces the definition of the Zener–Hollomon parameter and the constitutive equation of hyperbolic sine function. From Eq. (1), the value of Q can be defined as follows:

$$Q = R\left[\frac{\partial \ln \dot{\varepsilon}}{\partial \ln \sinh(\alpha\sigma)}\right] \cdot \left[\frac{\ln \sinh(\alpha\sigma)}{\partial(1/T)}\right]. \tag{2}$$

Fig. 2 indicates the variations of flow stress with strain rate and the reciprocal of temperature which are used to determine the value of Q according to Eq. (2). In this study, n was determined as 4.76 (= 1/0.21) and α was adjusted as 0.014 to make the data in Fig. 2(a) linear and parallel. Using the values of n and α, Q takes the average value of 435.3 kJ/mol.

To model the flow curves up to the peak, the Estrin and Mecking's method [19] which was based on the evolution of dislocation density due to concurrent work hardening and dynamic recovery (DRV) was used. In this approach, the evolution of dislocation density with strain is determined as the sum of differential hardening and softening terms as follows:

$$\frac{d\rho}{d\varepsilon} = \left(\frac{d\rho}{d\varepsilon}\right)^+ + \left(\frac{d\rho}{d\varepsilon}\right)^-. \tag{3}$$

Here, the first term stands for work hardening part and the second term the softening due to DRV. According to the Estrin and Mecking method [19] the terms in Eq. (3) can be replaced as follows:

$$\frac{d\rho}{d\varepsilon} = h - r\rho, \tag{4}$$

where h is the athermal work-hardening rate and r denotes the rate of dynamic recovery at a given temperature and strain rate. By doing some algebraic operations, the above differential equation can be written as follows describing a treatment of flow stress [20]:

$$\sigma = \left[\sigma_{\text{rec}}^2 - (\sigma_{\text{rec}}^2 - \sigma_0^2)exp(-r\varepsilon)\right]^{0.5}, \tag{5}$$

where σ_0 and σ_{rec} denote the initial and saturated stress defined as $(\alpha MGb)^2(h/r)$ and $(\alpha MGb)^2 \rho_0$, respectively. α is a shape factor in the order of unity, M is the Taylor factor (3.07 for FCC materials), G is the shear modulus, b is the magnitude of Burger's vector and ρ_0 is the initial dislocation density. We can take this simplifying assumption that ρ_0 is nearly negligible as compared to the stored dislocation density during hot deformation. This assumption is also more pertinent to a low SFE material such as austenite characterized by a sluggish DRV. Therefore, in the formulation of flow curve using Eq. (5), σ_0 can be neglected and the simplified description of work hardening curve can be as follows:

$$\sigma = \sigma_{\text{rec}}(1 - \exp(-r\varepsilon))^{0.5}. \tag{6}$$

The differentiation of which gives:

$$\frac{d\sigma}{d\varepsilon} = 0.5\sigma_{\text{rec}} r \exp(-r\varepsilon)(1 - \exp(-r\varepsilon))^{-0.5}. \tag{7}$$

Substituting $1-(\sigma/\sigma_{\text{rec}})^2$ for $\exp(-r\varepsilon)$, Eq. (7) can be written as:

$$\frac{d\sigma}{d\varepsilon} = 0.5r\left(\frac{\sigma_{\text{rec}}^2 - \sigma^2}{\sigma}\right). \tag{8}$$
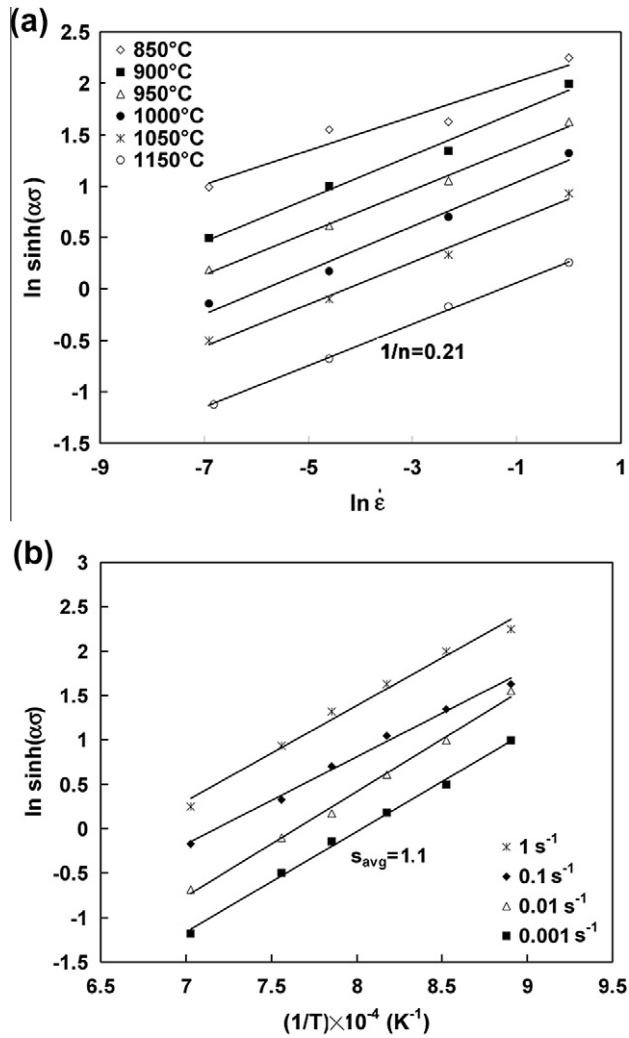
Fig. 2. Variation of the hyperbolic sine function of peak stress with, (a) strain rate and (b) the reciprocal of temperature for the determination of apparent activation energy according to Eq. (2).
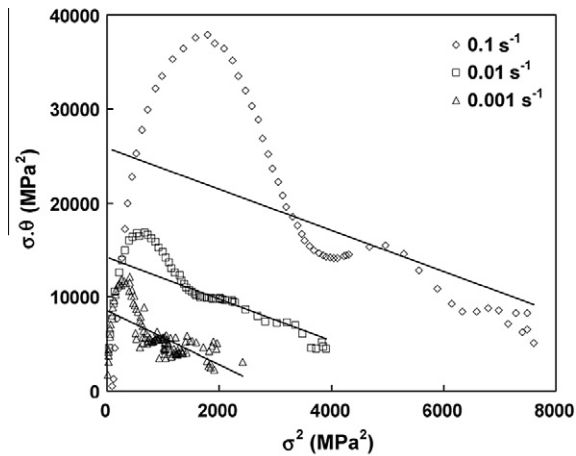

Fig. 3. Flow stress multiplied by work hardening rate versus the square of flow stress at 1050 °C used to determine the recovery factor and the DRV saturation stress.
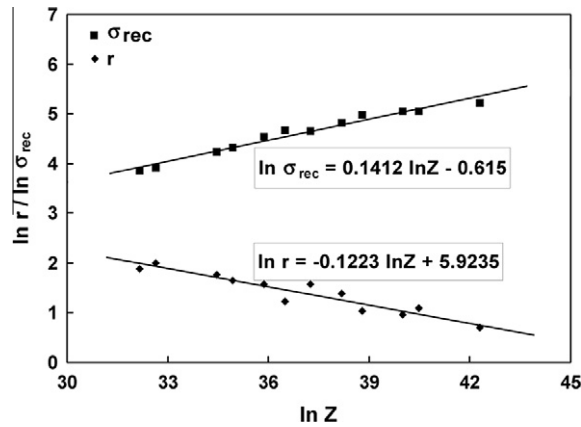
Fig. 4. Variation of dynamic recovery coefficient, r, and the saturation stress of DRV, σ_{rec} with the Zener-Hollomon parameter.

The plots of $\sigma \cdot \theta (=\sigma d\sigma/d\varepsilon)$ vs. σ^2, typically shown in Fig. 3, are linearly fitted according to Eq. (8) from which the slope and the intercept are therefore tantamount to $-0.5\,r$ and $0.5\,r\sigma_{rec}^2$, respectively. R and σ_{rec} values determined by the method mentioned are depicted versus the Z parameter in Fig. 4. The decrease in r and the concurrent increase in the saturation stress of DRV, σ_{rec}, with increasing Z reflect that DRV becomes less efficient as strain rate increases or temperature declines. Using the determined values for r and σ_{rec}, the predicted flow curves are depicted versus the experimental ones in Fig. 5. It manifests that the DRV model can give a good approximation of the actual flow curve up to the peak point of DRX flow curve. However, at strain close to the peak deviation in the model begin to appear. This can be attributed to the softening due to DRX which actually starts at a critical strain near the peak. Between the critical point and the peak both DRV and DRX occur. The situation has been further discussed elsewhere [20]. After the peak DRX occurs preferentially and therefore a model describing the nucleation and growth of new recrystallized grains should be adopted. The starting point of DRX can be therefore distinguished by studying the variation of work hardening rate versus flow stress as described by Poliak and Jonas [21]. The method proposed by Poliak and Jonas was used to characterize the critical points of the flow curves and to establish a relation between the characteristic points and the deformation variables, i.e. temperature and strain rate, incorporated in the Z parameter. In Fig. 6 the onset of DRX in the typical flow curves can be identified as the inflection point of the $\theta - \sigma$ curve near the saturated or peak stress. The observed inflection in the $\theta - \sigma$ curves is associated with the softening due to the first bulges of grain boundaries at the early stages of DRX. Beyond the peak, work hardening rate becomes increasingly minus due to the softening of DRX up to a maximum and then tends to zero again at the onset of the steady state flow. All the characteristic points are now discernible. Due to the influence of deformation condition on the kinetics of DRV and DRX, the positions of characteristic points are functions of the Zener–Hollomon parameter. DRX is shifted to higher strains when deformation temperature declines or strain rate increases. Therefore, characteristic strains and stresses are expected to increase as Z rises. The results showed that the critical strain, ε_c, is about 0.8 times the peak strain, ε_p, and the critical stress, σ_c, is about 0.98 times the peak stress, σ_p. It is also evident that the stress and strain required for the steady state deformation
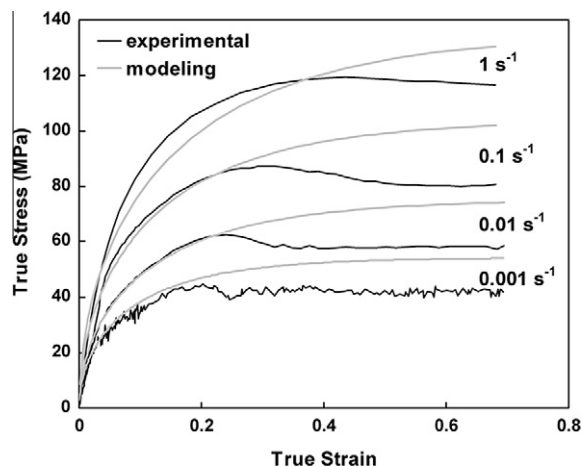

Fig. 5. Predicted flow curves indicating the accuracy of the Estrin and Mecking's equation to model the DRV region of flow curves at 1050 °C.
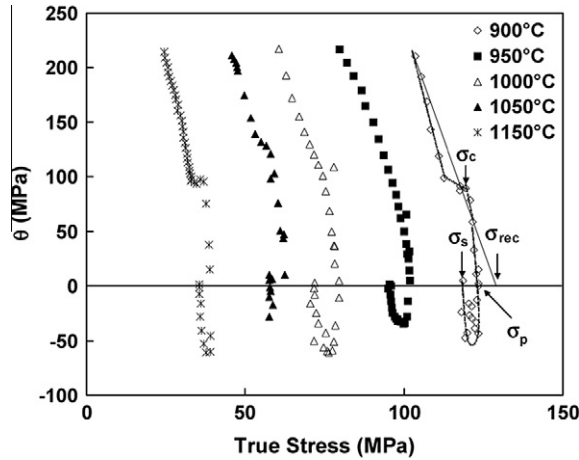
Fig. 6. Plot of work hardening rate vs. flow stress at different temperatures and strain rate of 0.01 s^{-1} used to determine the starting point of DRX, the peak stress and the steady state stress.

increases as Z rises. Depending on the results indicated in Fig. 7, the following power-law equations can simply correlate the characteristic strains and stresses to deformation condition:

$$\varepsilon = 0.008Z^{0.1},$$ (9)

$$\sigma_p = 0.78Z^{0.13},$$ (10)

$$\varepsilon_s = 0.004Z^{0.13},$$ (11)

$$\sigma_s = 0.36Z^{0.15}.$$ (12)

The developed power-law equations are very useful when modeling the DRX flow curve based on the Avrami's equation. Previous researchers have proposed that the kinetics of DRX bears the following relation with strain beyond the critical strain [22]:

$$X_{DRX} = 1 - \exp\left[-k(\varepsilon - \varepsilon_c)^n\right],$$ (13)

where n is the Avrami's power and k is a constant. The fractional softening due to DRX at the peak point of flow curve is known to be constantly about 10% [20] and further softening actually occurs between ε_p and ε_s. Therefore, the fractional softening between the peak and the onset of steady state flow can be written as follows:

$$X_{DRX}]_{\varepsilon_p}^{\varepsilon_s} = 0.9 - \exp\left[-k(\varepsilon - \varepsilon_p)^n\right].$$ (14)

Softening between the peak and the plateau can be also interpreted in terms of the decrease in flow stress as follows:

$$X_{DRX}]_{\varepsilon_p}^{\varepsilon_s} = \frac{\sigma_p - \sigma}{\sigma_p - \sigma_s}.$$ (15)

Combination of Eqs. (14) and (15) is given as follows:

$$\frac{\sigma_p - \sigma}{\sigma_p - \sigma_s} = 0.9 - \exp\left[-k(\varepsilon - \varepsilon_p)^n\right].$$ (16)

In order to determine the value of n and k, the plot of $\ln\ln(1/(0.9 - X_{DRX})$ determined from the stress term in Eq. (15) should be drawn versus $\ln(\varepsilon - \varepsilon_P)$ as indicated in Fig. 8. As expected, The experimental data can be linearly fitted according to Eq. (16) to determine n and k respectively as the slope and intercept. The average of slopes determines the Avrami exponent around 1.9 which is in good agreement with value of 2 reported for discontinues DRX in different alloys [23]. However, as indicated in Fig. 9, n and k actually decrease as Z value rises. These observations are in agreement with other reports on the dynamic recrystallization of other steel grades [13,23]. The reason is that when Z increases the rate of DRX decreases and therefore is completed at higher strains. The substitution of Eqs. (9)–(12) for the corresponding terms in Eq. (16) gives rise to a formalism of flow stress. Fig. 10 shows the results of modeling by Eq. (16). It is observed that the flow softening due to DRX is well predicted using the modified form of Avrami equation proposed in Eq. (16).
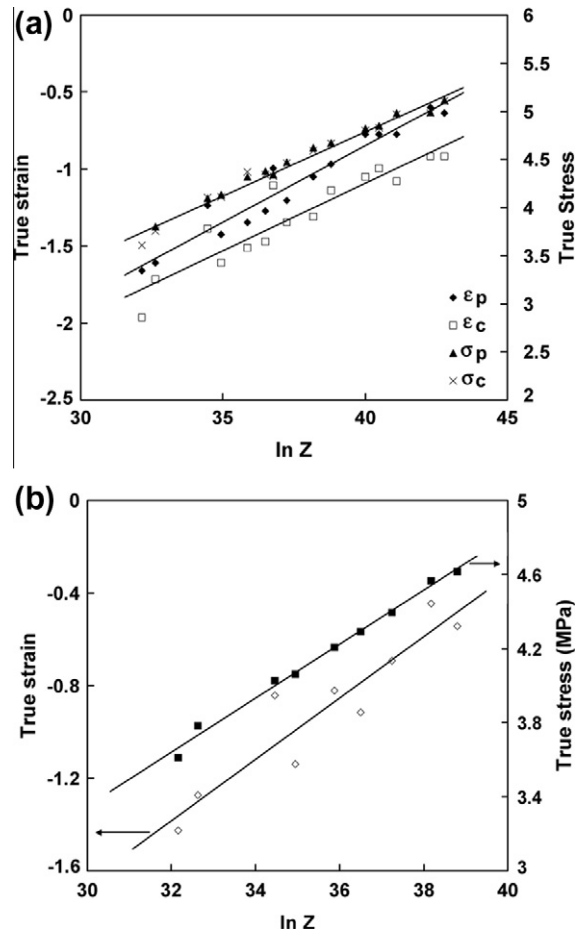
Fig. 7. Dependence of (a) the peak and critical strain and stress and (b) steady state strain and stress on the Z parameter.
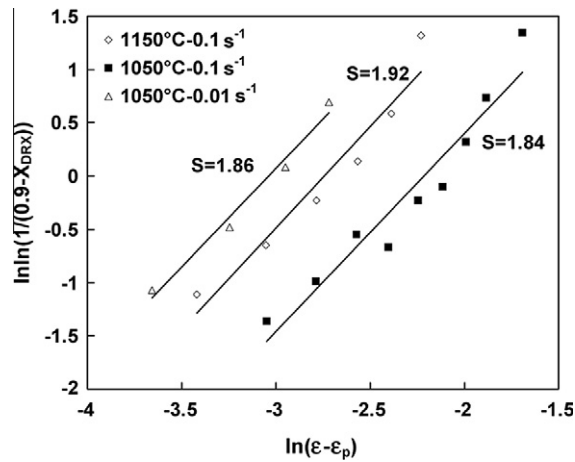

Fig. 8. Avrami graphs at different deformation conditions for the determination of n and k.

4. Conclusions

The hot working behavior of VCN200 medium carbon low alloy steel was analyzed by constitutive analysis as well as by modeling the flow curve. The most important results are drawn as follows:
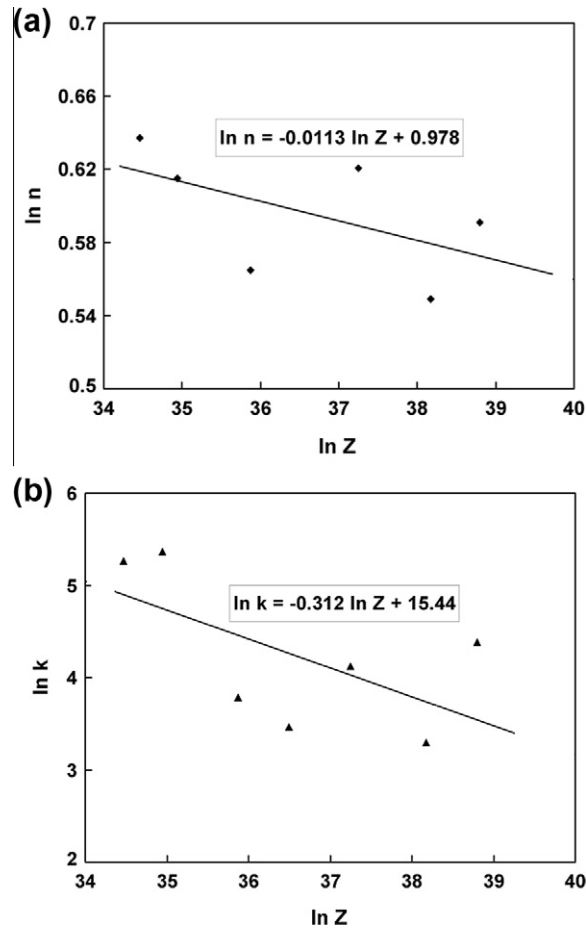
Fig. 9. Variation of (a) n and (b) k with the with Zener–Hollomon parameter.
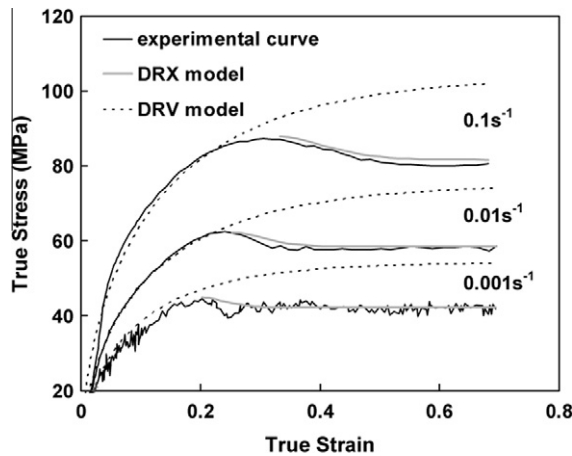

Fig. 10. Comparison of typical experimental flow curves obtained at 1050 °C and those obtained from the modeling of DRX and DRV regions.

(1) Dynamic recrystallization is the major microstructural phenomenon during hot working over temperature range of 900–1150 °C and strain rates of 0.001–1 s^{-1}.

(2) The constitutive analysis using the hyperbolic sine function can be performed and the value of apparent activation energy for the hot deformation is about 435 kJ/mol.

(3) The flow curves can be modeled using a dynamic recovery model with a good accuracy. All the factors in this model are defined in terms of the Zener–Hollomon parameter.

(4) A model can also be developed based on a modified Avrami's equation to estimate the fractional softening of DRX for any given strain in flow curve. The flow curve can be successfully predicted and generalize to different deformation conditions.

References

[1] H. Mirzadeh, J.M. Cabrera, J.M. Prado, A. Najafizadeh, Hot deformation behavior of a medium carbon microalloyed steel, Mater. Sci. Eng. A 528 (2011) 3876–3882.
[2] A. Momeni, A. Shokuhfar, S.M. Abbasi, Dynamic recrystallization of a Cr–Ni–Mo–Cu–Ti–V precipitation hardenable stainless steel, J. Mater. Sci. Tech. 23 (2007) 775–778.
[3] A. Momeni, K. Dehghani, Characterization of hot deformation behavior of 410 martensitic stainless steel using constitutive equations and processing maps, Mater. Sci. Eng. A527 (2010) 5467–5473.
[4] M. Meysami, S.A.A. Akbari Mousavi, Study on the behavior of medium carbon vanadium microalloyed steel by hot compression test, Mater. Sci. Eng. A527 (2010) 3049–3055.
[5] A. Momeni, S.M. Abbasi, Effect of hot working on flow behavior of Ti–6Al–4V alloy in single phase and two phase regions, Mater. Des. 31 (2010) 3599–3604.
[6] G.R. Johnson, W.H. Cook, A constitutive model and data for metals subjected to large strains, high strain rates and high temperatures, in: Proceedings of the Seventh International Symposium on Ballistics, Hague, Netherlands, 1983, pp. 541–547.
[7] S.I. Kim, Y. Lee, S.M. Byon, Study on constitutive relation of AISI 4140 steel subject to large strain at elevated temperatures, J. Mater. Process. Technol. 140 (2003) 84–89.
[8] A.H. Meysarni, R. Ghasemzadeh, S.H. Seyedein, M.R. Aboutalebi, R. Ebrahirni, M. Javidani, Physical simulation of hot deformation and microstructural evolution for 42CrMo4 steel prior to direct quenching, J. Iron Steel Res. Int. 16 (2009) 47–51.
[9] A. Momeni, H. Arabi, A. Rezaei, H. Badri, S.M. Abbasi, Study on constitutive relation of AISI 4140 steel subject to large strain at elevated temperatures, Mater. Sci. Eng. A528 (2011) 2158–2163.
[10] J.H. Bianchi, L.P. Karjalainen, Modelling of dynamic and metadynamic recrystallisation during bar rolling of a medium carbon spring steel, J. Mater. Process. Technol. 160 (2005) 267–277.
[11] S. Mandal, A.K. Bhaduri, V. Subramania Sarma, A study on microstructural evolution and dynamic recrystallization during isothermal deformation of a Ti-modified austenitic stainless steel, Met. Mater. Trans. 42A (2011) 1062–1072.
[12] A. Momeni, K. Dehghani, Prediction of dynamic recrystallization kinetics and grain size for 410 martensitic stainless steel during hot deformation, Met. Mater. Int. 16 (2010) 843–849.
[13] A. Momeni, K. Dehghani, G.R. Ebrahimi, H. Keshmiri, Modeling the flow curve characteristics of 410 martensitic stainless steel under hot working condition, Metall. Mater. Trans. 41A (2010) 2898–2904.
[14] W. Roberts, B. Ahlblom, A nucleation criterion for dynamic recrystallization during hot working, Acta Mater. 26 (1978) 801–813.
[15] R. Ding, Z.X. Guo, Coupled quantitative simulation of microstructural evolution and plastic flow during dynamic recrystallization, Acta. Mater. 49 (2001) 3163–3175.
[16] A. Momeni, S.M. Abbasi, A. Shokuhfar, Hot compression behavior of as-cast precipitation-hardening stainless steel, J. Iron Steel Res. Int. 14 (2007) 66–70.
[17] G.R. Ebrahimi, H. Keshmiri, A. Momeni, M. Mazinani, Dynamic recrystallization behavior of a superaustenitic stainless steel containing 16% Cr and 25% Ni, Mater. Sci. Eng. A, doi:10.1016/j.msea.2011.05.081.
[18] J.J. Jonas, T. Sakai, A new approach to dynamic recrystallization, in: G. Krauss (Ed.), ASM Materials Science Seminar, Deformation Processing And Structure, 23–24 Oct., 1982, Missouri, USA, pp. 185–228.
[19] Y. Estrin, H. Mecking, A unified phenomenological description of work hardening and creep based on one-parameter models, Acta Metal. 32 (1984) 57–70.
[20] A. Momeni, K. Dehghani, G.R. Ebrahimi, Modeling the initiation of dynamic recrystallization using a dynamic recovery model, J. Alloys Comp., doi:10.1016/j.jallcom.2011.07.014.
[21] E.I. Poliak, J.J. Jonas, Initiation of dynamic recrystallization in constant strain rate hot deformation, ISIJ Int. 43 (2003) 684–691.
[22] W. Roberts, Dynamic changes that occur during hot working and their significance regarding microstructural development and hot workability, in: G. Krauss (Ed.), ASM Materials Seminar, deformation processing and structure, 23-24 Oct., 1982, Missouri, USA, pp. 109–184.
[23] G.E. Dieter, H.A. Kuhn, S.L. Semiatin (Eds.), Handbook of Workability and Process Design, ASM, Materials Park, Ohio, 2003, pp. 35–44.